

Control-aware Learning of Koopman Embedding Models

Daisuke Uchida¹ and Karthik Duraisamy¹

Abstract—A learning method is proposed for Koopman operator-based models with the goal of improving closed-loop control behavior. A neural network-based approach is used to discover a space of observables in which nonlinear dynamics is linearly embedded. While accurate state predictions can be expected with the use of such complex state-to-observable maps, undesirable side-effects may be introduced when the model is deployed in a closed-loop environment. This is because of modeling or residual error in the linear embedding process, which can manifest itself in a different manner compared to the state prediction. To this end, a technique is proposed to refine the originally trained model with the goal of improving the closed-loop behavior of the model while retaining the state-prediction accuracy obtained in the initial learning. Finally, a simple data sampling strategy is proposed to use inputs deterministically sampled from continuous functions, leading to additional improvements in the controller performance for nonlinear dynamical systems. Several numerical examples are provided to show the efficacy of the proposed method.

I. INTRODUCTION

The Koopman operator describes the evolution of a nonlinear dynamical system in terms of a possibly infinite-dimensional but linear operator in a lifted space of observables. Starting from applications in dimension reduction of high-dimensional nonlinear systems such as turbulent flows [1], [2], the Koopman operator has gained high popularity in recent years as a data-driven modeling approach for dynamical systems. Among a number of applications is that of data-driven control. On the basis of finite-dimensional approximation of the Koopman operator derived from Extended Dynamic Mode Decomposition (EDMD) [3], which yields a Linear Time-Invariant (LTI) data-driven model, several linear controllers have been applied such as Linear Quadratic Regulator (LQR) [4]–[6] and Model Predictive Control (MPC) [7]–[11]. Also, to overcome a limitation of the Koopman formalism that the modeling error is practically inevitable due to the nature of purely data-driven modeling procedures, several concepts from control theories, e.g., robust tube-based MPC [11], offset-free MPC [12], conformant synthesis [13], and so on, have been utilized to achieve the control objectives in the fully data-driven setting. While there are many frameworks and methods in literature to incorporate the Koopman operator into data-driven control, not much attention has been paid to the modeling aspect of the Koopman operator-based framework itself, i.e., how the modeling error behaves while implementing state-prediction or feedback control, which pertains to practically unavoidable discrepancy between theories and actual implementations and should be considered as an essential factor for reliable modeling procedures and control applications.

It has been recognized that the convergence property of the EDMD algorithm [14] does not hold for non-autonomous types of Koopman models [7]. This motivates the use of

neural networks to learn the observable functions themselves along with the finite-dimensional approximation of the Koopman operator. Especially, while the model structure we employ in this paper is restrictive so that we can realize LTI systems in the embedded space, which allows the use of linear controller designs even if the dynamics is nonlinear, it is shown that obtaining high state-predictive accuracy is achievable if the dynamics is linear with respect to input and one has access to enough data and computational resources that afford high-dimensional and complex feature maps.

On the other hand, we show that the modeling error of the Koopman models interacts with the closed-loop system in a different way from the state-prediction and we exemplify that the controller performance can greatly suffer from the modeling error, on which the complexity and dimension of observables have a large influence. To improve the possibly undesirable closed-loop behavior induced by Koopman-based control models, a control-aware method is proposed, in which the model is refined after the initial training with additional use of data points sampled from closed-loop dynamics. This modification of the model aims to directly reduce the impact of the modeling error on the controller performance. Moreover, with the same intent as the control-aware learning method, we also present a simple yet effective data sampling strategy that only uses inputs deterministically sampled from continuous functions.

This paper is organized as follows. In Section II, the Koopman operator framework for non-autonomous systems is presented. In Section III, we discuss the manifestation of the modeling error on both prediction and control and propose a control-aware learning method along with a data sampling strategy about inputs to improve the actual closed-loop behavior. Finally, several dynamical systems are tested to show the effectiveness of the proposed method in Section IV.

II. KOOPMAN OPERATOR THEORY FOR NON-AUTONOMOUS SYSTEMS

A. Koopman Operator for General Non-Autonomous Systems

In this section, the Koopman operator is formally introduced for general non-autonomous systems, which forms the basis of observations made in Section III and the proposed method. Consider a dynamical system:

$$\dot{x}(t) = f(x(t), u(t)), \quad (1)$$

where $x(t) \in \mathcal{X} \subseteq \mathbb{R}^n$, $u(t) \in \mathcal{U} \subseteq \mathbb{R}^p$, and $f : \mathcal{X} \times \mathcal{U} \rightarrow \mathbb{R}^n$ are the state, the input, and the possibly nonlinear mapping describing dynamics of the system, respectively. Throughout the paper, we assume the solution $x(t)$ to (1) to be continuous with respect to t . With a first-order time discretization, (1) yields the following difference equation:

$$x_{k+1} = F(x_k, u_k), \quad (2)$$

¹The authors are with the department of Aerospace Engineering, University of Michigan, Ann Arbor, Michigan, 48109, USA (e-mail: duchida@umich.edu, kdur@umich.edu).

where $x_k := x(k\Delta t)$, $u_k := u(k\Delta t)$, and Δt denotes the sampling period. On the assumption $\Delta t \ll 1$, we consider (2) as the discrete-time system whose dynamics is equivalent to that of (1). It is assumed that f (i.e., F) is unknown and its dynamics is modeled in a data-driven manner.

In the Koopman operator formalism, the dynamics is characterized through functions called observables, which are mappings from the state-space into \mathbb{R} . While the Koopman operator was first introduced in the context of autonomous systems, there have been also several efforts extending it to non-autonomous systems with control inputs [7], [15], [16]. In a formal extension [7], the state-space is extended to the augmented space $\mathcal{X} \times l(\mathcal{U})$, where

$$l(\mathcal{U}) := \{\mathbf{U} := (u_1, u_2, \dots) \mid u_i \in \mathcal{U}, \forall i \in \mathbb{N}\}, \quad (3)$$

is the space of sequences of inputs, and the observables g are of the form:

$$g : \mathcal{X} \times l(\mathcal{U}) \rightarrow \mathbb{R} : (x_k, \mathbf{U}) \mapsto g(x_k, \mathbf{U}). \quad (4)$$

In practice, the observables g may be considered as the feature maps that are either specified by users or learned from data in the modeling procedure.

The Koopman operator corresponding to the non-autonomous system (2) is defined as an infinite-dimensional linear operator $\mathcal{K} : \mathcal{F} \rightarrow \mathcal{F}$ (\mathcal{F} : space of functions g) s.t.

$$\mathcal{K}g = g \circ \hat{F} \Leftrightarrow (\mathcal{K}g)(x_k, \mathbf{U}) = g(\hat{F}(x_k, \mathbf{U})), \quad (5)$$

where the mapping $\hat{F} : \mathcal{X} \times l(\mathcal{U}) \rightarrow \mathcal{X} \times l(\mathcal{U})$ is defined by

$$\hat{F}(x_k, \mathbf{U}) := (F(x_k, u_k), \mathcal{S}\mathbf{U}) = (x_{k+1}, \mathcal{S}\mathbf{U}), \quad (6)$$

with the notation $\mathbf{U} = (u_k, u_{k+1}, \dots)$, and \mathcal{S} denotes the shift operator s.t.

$$\mathcal{S}\mathbf{U} = \mathcal{S}(u_k, u_{k+1}, \dots) := (u_{k+1}, u_{k+2}, \dots). \quad (7)$$

It is easily inferred from (5) that \mathcal{K} is a linear operator. Note that since (2) only specifies the evolution of x_k , it is required to introduce the sequence $\mathbf{U} = (u_k, u_{k+1}, \dots)$ of inputs, which can be also interpreted as an input signal (i.e., a function) $U : \mathbb{Z}_{\geq 0} \rightarrow \mathcal{U}$, to formally define the Koopman operator \mathcal{K} . The equation (5) along with the definition (6) can be viewed as the evolution of the dynamics (2) through the observables g .

B. Finite Dimensional Approximation of the Koopman Operator and Data-Driven Koopman Models

To apply the Koopman operator formalism to dynamical systems modeling, a finite-dimensional approximation K of the Koopman operator \mathcal{K} is introduced as follows.

Proposition 1: Given observables $g_i \in \mathcal{F}$ ($i = 1, \dots, D$), let g be an arbitrary element of $\text{span}(g_1 \dots, g_D)$. Then, $\mathcal{K}g \in \text{span}(g_1 \dots, g_D)$, i.e., $\text{span}(g_1 \dots, g_D)$ is an invariant subspace under the action of the Koopman operator $\mathcal{K} : \mathcal{F} \rightarrow \mathcal{F}$, if and only if there exists $K \in \mathbb{R}^{D \times D}$ s.t.

$$[\mathcal{K}g_1 \dots \mathcal{K}g_D]^\top = K[g_1 \dots g_D]^\top. \quad (8)$$

Proof: See Appendix A. ■

From an engineering perspective, it is of great interest to introduce the observables such that they allow practical models for control applications. One major choice of g_i for the Koopman control problem takes the following structure

of observables [10], [11], [17]:

$$[g_1(x_k, \mathbf{U}) \dots g_D(x_k, \mathbf{U})]^\top = [x_k^\top \tilde{g}(x_k)^\top u_k^\top]^\top, \quad (9)$$

where $D = n + N + p$ and $\tilde{g}(x_k) \in \mathbb{R}^N$ represents a vector-valued function from \mathcal{X} into \mathbb{R}^N for some $N \in \mathbb{N}$. Note that only the first element u_k in the sequence $\mathbf{U} = (u_k, u_{k+1}, \dots)$ appears in the definition (9), which leads to a practical form of data-driven models consistent with many linear controller designs such as LQR and MPC. On the assumption that we have access to x_k and u_k as data, we consider the following finite-dimensional approximation $K_c \in \mathbb{R}^{(n+N+p) \times (n+N+p)}$ of the Koopman operator \mathcal{K} :

$$\begin{bmatrix} x_{k+1} \\ \tilde{g}(x_{k+1}) \\ u_{k+1} \end{bmatrix} \approx \underbrace{\begin{bmatrix} A & B \\ & * \end{bmatrix}}_{=: K_c} \begin{bmatrix} x_k \\ \tilde{g}(x_k) \\ u_k \end{bmatrix}, \quad (10)$$

where matrices $A \in \mathbb{R}^{(n+N) \times (n+N)}$ and $B \in \mathbb{R}^{(n+N) \times p}$ are to be learned along with the feature maps \tilde{g} . Note that (10) is approximate since $\text{span}(g_1, \dots, g_D)$ defined by (9) may not be invariant under the action of \mathcal{K} .

Noticing that the first $n + N$ rows of (10) are enough to specify the evolution of the state x_k s.t.

$$\begin{bmatrix} x_{k+1} \\ \tilde{g}(x_{k+1}) \end{bmatrix} \approx A \begin{bmatrix} x_k \\ \tilde{g}(x_k) \end{bmatrix} + Bu_k, \quad (11)$$

we are only interested in learning (11) and the last p rows of K_c in (10) are ignored in the preceding formulations. The discarded equations approximately represent u_{k+1} given x_k and u_k , which corresponds to the fact that the Koopman operator shifts the sequence of inputs according to (7). From (11), the modeling error is defined as:

$$r(x, u) := \begin{bmatrix} F(x, u) \\ \tilde{g}(F(x, u)) \end{bmatrix} - \left(A \begin{bmatrix} x \\ \tilde{g}(x) \end{bmatrix} + Bu \right), \quad (12)$$

and its norm:

$$\|r\|_{L_2} = \sqrt{\int_{\mathcal{X} \times \mathcal{U}} \|r(x, u)\|_2^2 dx du}, \quad (13)$$

may be used as a characteristic to evaluate the model, e.g., (11) is exact almost everywhere if (13) is well-defined and $\|r\|_{L_2} = 0$.

The model (11) is an LTI system in the new coordinates $[x_k^\top \tilde{g}(x_k)^\top]^\top$ and linear controller designs can be applied to control (2). In this paper, the following feedback controller with a static gain $\mathbf{K} \in \mathbb{R}^{p \times (n+N)}$ is considered:

$$u_k = \mathbf{K}[x_k^\top \tilde{g}(x_k)^\top]^\top. \quad (14)$$

III. CONTROL-CONSISTENT LEARNING OF KOOPMAN EMBEDDING

A. Motivating Example

We consider the following one-dimensional system as a guiding example to motivate the proposed control-aware learning.

$$x_{k+1} = x_k^2 e^{-x_k} + u_k, \quad x_k, u_k \in \mathbb{R}. \quad (15)$$

Suppose that we create the Model 1 defined as:

$$\begin{bmatrix} x_{k+1} \\ x_{k+1}^2 e^{-x_{k+1}} \end{bmatrix} \approx A \begin{bmatrix} x_k \\ x_k^2 e^{-x_k} \end{bmatrix} + Bu_k, \quad (\tilde{g}(x_k) = x_k^2 e^{-x_k}). \quad (16)$$

From Proposition 2 in Section III-D, perfect state prediction with no error is possible with A and B given as the following forms:

$$A = \begin{bmatrix} 0 & 1 \\ \alpha_1 & \alpha_2 \end{bmatrix}, B = \begin{bmatrix} 1 \\ \alpha_3 \end{bmatrix}, \alpha_i \in \mathbb{R}. \quad (17)$$

The modeling error (12) is then represented by

$$r(x_k, u_k) = \begin{bmatrix} 0 \\ (x_k^2 e^{-x_k} + u_k)^2 \exp(-x_k^2 e^{-x_k} - u_k) \\ -\alpha_1 x_k - \alpha_2 x_k^2 e^{-x_k} - \alpha_3 u_k \end{bmatrix}. \quad (18)$$

Suppose we also have the Model 2, which has richer features:

$$\begin{bmatrix} x_{k+1} \\ x_{k+1}^2 e^{-x_{k+1}} \\ x_{k+1}^2 \end{bmatrix} \approx A \begin{bmatrix} x_k \\ x_k^2 e^{-x_k} \\ x_k^2 \end{bmatrix} + B u_k, \left(\tilde{g}(x_k) = \begin{bmatrix} x_k^2 e^{-x_k} \\ x_k^2 \end{bmatrix} \right). \quad (19)$$

Perfect state prediction can be also achieved with

$$A = \begin{bmatrix} 0 & 1 & 0 \\ \beta_1 & \beta_2 & \beta_3 \\ \beta_4 & \beta_5 & \beta_6 \end{bmatrix}, B = \begin{bmatrix} 1 \\ \beta_7 \\ \beta_8 \end{bmatrix}, \beta_i \in \mathbb{R}. \quad (20)$$

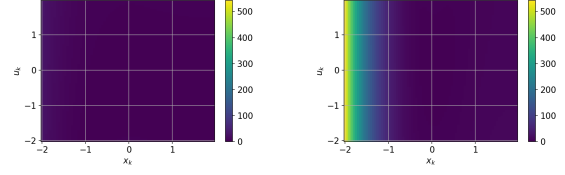
In this case, however, the modeling error $r(x_k, u_k)$ takes a different form:

$$r(x_k, u_k) = \begin{bmatrix} 0 \\ (x_k^2 e^{-x_k} + u_k)^2 \exp(-x_k^2 e^{-x_k} - u_k) \\ -\beta_1 x_k - \beta_2 x_k^2 e^{-x_k} - \beta_3 x_k^2 - \beta_7 u_k \\ (x_k^2 e^{-x_k} + u_k)^3 - \beta_5 x_k \\ -\beta_6 x_k^2 e^{-x_k} - \beta_7 x_k^2 - \beta_8 u_k \end{bmatrix}. \quad (21)$$

Figures 1a and 1b show the heat maps of $\|r(x_k, u_k)\|_2$, where the model parameters α_i and β_i are obtained by EDMD [7]. Model 2 in (19) is highly erroneous for $x_k < 0$ compared to the Model 1 in (16) and the modeling error accumulates according to (38) in Section III-D leading to undesirable closed-loop behaviors. Figure 1c shows the controller performance of both models, where K in (14) is computed as an LQR gain with the cost function $\sum_{k=0}^{\infty} x_k^2 + u_k^2$. Despite the fact that both models achieve precisely zero state-prediction error, the controller designed for Model 2 causes an undesirable oscillation even as the open-loop dynamics quickly converges to the origin after $k = 1$. Herein, it is also emphasized that from the state-prediction point of view, complex and large models such as the Model 2 may be preferable in general since it is more likely to achieve better state-prediction by Corollary 1 in Section III-D. To deal with this degradation of the controller performance, which is not revealed from the state-prediction accuracy, a control-aware learning approach is proposed along with a simple data sampling strategy.

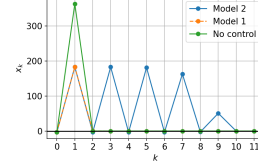
B. Modeling Errors of Koopman Control Models

Several methods have been proposed to learn the model (11), among of which the most straightforward one is to first specify the feature maps \tilde{g} and infer A and B from data. This is reduced to a linear regression problem and a unique solution can be obtained in the same manner as the Dynamic Mode Decomposition (DMD) [1], [2]. This learning algorithm with nonlinear observables is called the Extended Dynamic Mode Decomposition (EDMD) [3], based on which many data-driven Koopman controller designs



(a) Model 1 (18).

(b) Model 2 (21).



(c) Control simulations.

Fig. 1: (a), (b): Heat maps of $\|r(x_k, u_k)\|_2$. (c): Controller performance with $x_0 = -3.4298$.

are developed [5]–[11], [17]–[19]. An important feature of the EDMD algorithm is its convergence property. Letting $\mathcal{F} = L_2(\mathcal{X} \times l(\mathcal{U}))$, the approximation obtained by EDMD is, under several assumptions, shown to converge to the true Koopman operator in the strong operator topology as the number M of data points and the number D of observables g_i tend to infinity [14], [20]. Specifically, this convergence property is stated as follows: for $\forall g \in L_2(\mathcal{X} \times l(\mathcal{U}))$,

$$\lim_{D \rightarrow \infty} \int_{\mathcal{X} \times l(\mathcal{U})} |(P_D^\mu \mathcal{K}) P_D^\mu g - \mathcal{K}g|^2 d\mu = 0, \quad (22)$$

where P_D^μ and μ are the L_2 projection onto $\text{span}(g_1, \dots, g_D)$ and a measure with which $L_2(\mathcal{X} \times l(\mathcal{U}))$ is endowed, respectively. The operator $P_D^\mu \mathcal{K}$ in (22) is related to the finite dimensional approximation K computed by EDMD in the following manner:

$$\lim_{M \rightarrow \infty} \|a^\top K [g_1 \cdots g_D]^\top - P_D^\mu \mathcal{K}g\| = 0, \quad \forall g = a^\top [g_1 \cdots g_D]^\top \in \text{span}(g_1, \dots, g_D), a \in \mathbb{R}^D, \quad (23)$$

where $\|\cdot\|$ is an arbitrary norm on $\text{span}(g_1, \dots, g_D)$. The convergence property (22) implies that data-driven Koopman models can provide reasonable approximation with sufficiently large M and D . However, it is not the case for non-autonomous systems as seen in the following remark.

Remark 1: Given feature maps $\tilde{g}(x_k)$, the approximation K_c in (10) does not possess the convergence property (22) since for (22) to hold, it is necessary that $\{g_i\}_{i=1}^D$ is an orthonormal basis of $L_2(\mathcal{X} \times l(\mathcal{U}))$ as $D \rightarrow \infty$ [14]. As described in [7], no elements of $\mathcal{U} = (u_k, u_{k+1}, \dots)$ except for the first one u_k depend on the definition (9) and it is obvious that they cannot form any basis of $L_2(\mathcal{X} \times l(\mathcal{U}))$.

No convergence property of the model (10) or (11) implies $\|r\|_{L_2}$ may not be negligibly small even if D and M are sufficiently large. To this end, we adopt another learning formulation, where the nonlinear feature maps \tilde{g} are also learned from data along with matrices A and B .

Step 1: (Initial Training)

Find $g, A \in \mathbb{R}^{(n+N) \times (n+N)}$, and $B \in \mathbb{R}^{(n+N) \times p}$ s.t.

$$\{g, A, B\} = \underset{\{g, A, B\}}{\operatorname{argmin}} J(g, A, B), \quad (24)$$

$$\text{where } J(g, A, B) := \lambda_1 \|AG_x + BU - G_y\|_F^2 + \lambda_2 \|W(AG_x + BU) - Y\|_F^2, \quad (25)$$

$$G_x := [g(x_1) \cdots g(x_M)], \quad U := [u_1 \cdots u_M],$$

$$G_y := [g(y_1) \cdots g(y_M)], \quad Y := [y_1 \cdots y_M],$$

$$y_k = F(x_k, u_k), \quad k = 1, \dots, M,$$

$$W := \begin{bmatrix} I & 0 \end{bmatrix}, \quad (26)$$

$$g: \mathcal{X} \rightarrow \mathbb{R}^{n+N} : x_k \mapsto \begin{bmatrix} x_k \\ \tilde{g}(x_k) \end{bmatrix}, \quad (27)$$

$$\tilde{g}(x_k) = \text{NN}(x_k; w) \text{ (a neural network)}. \quad (28)$$

C. Initial Training: Simultaneous Learning of the Feature Maps and the System Matrices

Another class of methods to learn model (11) estimates the system matrices A, B , and the feature maps \tilde{g} simultaneously. The resulting models are expected to achieve better predictive accuracy than those of the linear formulations such as EDMD since they can have greater model expressivity with the feature maps \tilde{g} also learned from data along with the matrices A and B . Especially, the use of neural networks has been shown to be promising to incorporate into the Koopman operator-based modeling, analyses, and control [21]–[25].

Hence, the proposed method characterizes the feature maps \tilde{g} in (11) as a neural network aiming at high predictive accuracy and solves a nonlinear regression problem to learn A, B , and \tilde{g} , which is formulated as Step 1.

The loss function $J(g, A, B)$ in (25) consists of two terms. The first one multiplied by a hyperparameter λ_1 accounts for (approximately) minimizing $\|r\|_{L_2}$ in (13). The other one with a hyperparameter λ_2 intends to directly minimize the state-reconstruction error by applying the decoder W to the model prediction in order to compare it with the state y_k . While the decoder may be also characterized by a neural network in general, the specific structure (9) of observables, which explicitly includes the state x_k , allows an analytical expression of the decoder W in (26).

The nonlinear feature maps \tilde{g} are defined as a fully-connected feed-forward neural network:

$$\text{NN}(x_k; w) := \sigma(\Theta_l \sigma(\cdots \Theta_2 \sigma(\Theta_1 x_k + b_1) + b_2 \cdots) + b_l), \quad (29)$$

$$w := \{\Theta_i, b_i\}_{i=1}^l, \quad (30)$$

where Θ_i, b_i , and σ are a kernel, a bias, and an activation function, respectively. In this paper, we only consider continuous activation functions so that (29) is continuous.

D. Second Training: Modification of the Initial Model

1) State-Prediction Accuracy:

Characterizing observables by a neural network allows greater expressivity, which can lead to higher accuracy of the data-driven model if the optimization problem is feasible. On the other hand, from the controller design perspective, including high-order nonlinearities in the observables is not preferable since it may introduce unexpected or undesirable

effect on the closed-loop system due to the modeling error, which could even alter the actual closed-loop system unstable, while it is easier for the state prediction to eliminate the modeling error. Specifically, the state prediction is implemented as follows:

$$x_{k+1}^{\text{est}} = \underbrace{[I \ 0]}_{=W} \left\{ A \begin{bmatrix} x_k^{\text{est}} \\ \tilde{g}(x_k^{\text{est}}) \end{bmatrix} + B u_k \right\}, \quad k = 0, 1, \dots, \quad (31)$$

where x_k^{est} denotes the state prediction at time k and $x_0^{\text{est}} = x_0$ is given. From (31), the modeling error in the state prediction is evaluated as:

$$x_{k+1} = [I \ 0] \left\{ A \begin{bmatrix} x_k \\ \tilde{g}(x_k) \end{bmatrix} + B u_k \right\} + [I \ 0] r(x_k, u_k). \quad (32)$$

Proposition 2: Let x_k and u_k be arbitrary. There exist $\tilde{g}, A_1 \in \mathbb{R}^{n \times n}, A_2 \in \mathbb{R}^{n \times N}$ and $B_1 \in \mathbb{R}^{n \times p}$ s.t.

$$F(x_k, u_k) = A_1 x_k + A_2 \tilde{g}(x_k) + B_1 u_k, \quad (33)$$

if and only if

$$[I \ 0] r(x_k, u_k) = 0, \quad (34)$$

i.e., (31) has no state prediction error.

Proof: Let $[A_1 \ A_2] \in \mathbb{R}^{n \times (n+N)}$ and $B_1 \in \mathbb{R}^{n \times p}$ be the first n rows of A and B in (32), respectively. From (2), the equation (32) reads

$$F(x_k, u_k) = A_1 x_k + A_2 \tilde{g}(x_k) + B_1 u_k + [I \ 0] r(x_k, u_k), \quad (35)$$

which implies the statement of the proposition. \blacksquare

Note that there exist \tilde{g}, A_1, A_2 , and B_1 that satisfy (33) with $A_2 = 0$ or $\tilde{g}(x_k) \equiv 0$ if and only if the original dynamics (2) is linear.

Corollary 1: If (2) is of the linear form w.r.t. input: $F(x_k, u_k) = \tilde{F}(x_k) + \tilde{B} u_k$ ($\tilde{B} \in \mathbb{R}^{n \times p}$), including an enough number of different features to reconstruct \tilde{F} is necessary and sufficient for (31) to be able to achieve zero state-prediction error. In case of control-affine dynamics s.t. $\tilde{B} = \tilde{B}(x_k)$ is dependent on x_k , the same argument holds if the state-prediction is implemented with $u_k \equiv 0$.

Although the specific model structure we adopt in (11) limits the validity of accurate state-prediction to certain classes of dynamics as seen in Corollary 1, it is considered as a preferable property from the controller design perspective since it allows to utilize linear systems theories in the new coordinates $[x_k^T \ \tilde{g}(x_k)^T]^T$ to control possibly nonlinear dynamics. However, it should be emphasized that the choice of model structure is a trade-off relation between the simple and practical controller designs and applicability of the method to actual nonlinear systems, i.e., such linear controller designs in the embedded space will result in poor control performance if the model has a large modeling error.

2) Accuracy in Terms of Closed-Loop Dynamics:

While the accuracy of the state prediction of the model (11) may be evaluated by Proposition 2, its accuracy in terms of controller design is characterized in a different way. Note that the system to be controlled by the feedback controller K in (14) is assumed to be a linear time-invariant system:

$$\xi_{k+1} = A \xi_k + B u_k, \quad \xi_k \in \mathbb{R}^{n+N}, \quad (36)$$

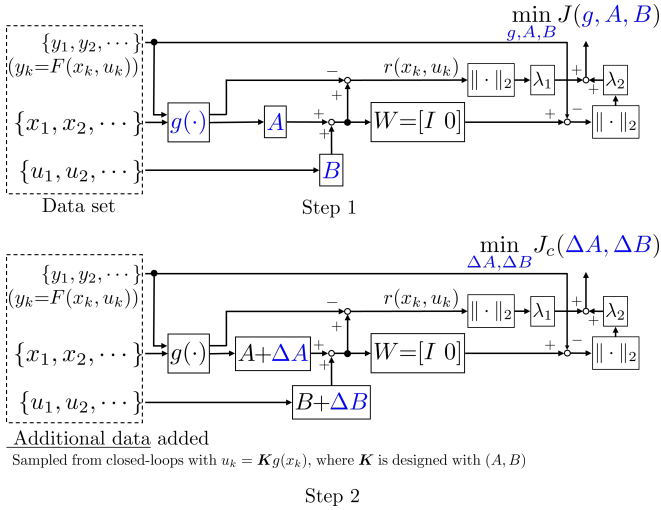


Fig. 2: Schematic of the learning procedure of the proposed method. In Step 2, constraints $\|\Delta A\| \leq \epsilon_A$ and $\|\Delta B\| \leq \epsilon_B$ are imposed.

and we can only ensure properties of the closed-loop system:

$$\xi_{k+1} = (A + BK)\xi_k = (A + BK)^{k+1}\xi_0. \quad (37)$$

Clearly, (36) is identical to the Koopman control model (11) if $\|r\|_{L_2} = 0$ and $\xi_0 = [x_0^T \tilde{g}(x_0)^T]^T$. However, in general cases where $r(x_k, u_k) \neq 0$, the modeling error may persist at any time and accumulate as follows:

$$\begin{aligned} \begin{bmatrix} x_{k+1} \\ \tilde{g}(x_{k+1}) \end{bmatrix} &= (A + BK)^{k+1} \begin{bmatrix} x_0 \\ \tilde{g}(x_0) \end{bmatrix} \\ &+ \sum_{i=0}^k (A + BK)^i r \left(x_{k-i}, K \begin{bmatrix} x_{k-i} \\ \tilde{g}(x_{k-i}) \end{bmatrix} \right), \end{aligned} \quad (38)$$

in which (14) is substituted. The second term of the r.h.s. of (38) represents the discrepancy between (36) and (11), which directly leads to degradation of controller performance. Since the error propagation in (38) reflects all components of $r(x_k, u_k)$ unlike the state prediction as in (32), the actual closed-loop system could greatly suffer from the modeling error depending on the design and/or the dimensions of \tilde{g} , as illustrated in the example of Section III-A.

In the proposed method, considering that the controller performance of the Koopman control model (11) can deteriorate due to the modeling error, the second training process formulated as Step 2 follows Step 1 in case the control objective is not achieved by the initially learned model. Specifically, data points sampled from a closed-loop system formed by (14), for which the initially learned A and B are used to design a controller, are added to the initial data set so that the second learning problem can directly minimize the modeling error in the regime of closed-loop dynamics (38).

The modification of the initial model is implemented by updating matrices A and B to $A + \Delta A$ and $B + \Delta B$, where we impose the constraint that the modified model retains dynamics close to the initial one. This constraint prevents the additional learning, which retrains the model with additional closed-loop data, from degrading the high

Step 2: (Modification of the initial model)

Given g, A, B , and a controller gain K that is designed with (A, B) , find ΔA and ΔB s.t.

$$\{\Delta A, \Delta B\} := \underset{\{\Delta A, \Delta B\}}{\operatorname{argmin}} J_c(\Delta A, \Delta B), \quad (39)$$

$$\text{subject to: } \|\Delta A\| \leq \epsilon_A, \quad (40)$$

$$\|\Delta B\| \leq \epsilon_B, \quad (41)$$

where

$$J_c(\Delta A, \Delta B) := \lambda_1 \|(A + \Delta A)G_x + (B + \Delta B)U - G_y\|_F^2 + \lambda_2 \|W((A + \Delta A)G_x + (B + \Delta B)U) - Y\|_F^2, \quad (42)$$

$$y_k = F(x_k, u_k),$$

and part of input data is generated by the feedback law $u_k = K g(x_k)$.

predictive accuracy obtained in the initial training. Specifically, ΔA and ΔB have the constraints that their induced 2-norms $\|\Delta A\| := \sup_{\|x\|=1} \|\Delta A x\|_2$ and $\|\Delta B\|$ are bounded by hyperparameters ϵ_A and ϵ_B , respectively. Finally, the controller gain is recomputed with the updated parameters $(A + \Delta A, B + \Delta B)$. The schematic of the learning procedure of the proposed method is shown in Fig. 2.

E. Characteristics to Measure the Accuracy

As stated in Proposition 1, the existence of an invariant subspace under the action of the Koopman operator is an essential factor for the modeling procedure, which determines if there exists a finite-dimensional model that can embed the original dynamics linearly in the subspace spanned by observables. In this regard, in addition to the modeling error defined in (12), one can also consider evaluating to what extent the subspace in which the model coordinates are defined is close to being invariant to measure the accuracy of modeling. Specifically, given some finite-dimensional subspace $\mathcal{F}_{\text{sub}} \subset \mathcal{F}$, it is obvious by Proposition 1 that if \mathcal{F}_{sub} is shown to be invariant under the action of \mathcal{K} , the realization of an exact model without any modeling error is possible with an arbitrary choice of observables from \mathcal{F}_{sub} . Also, finding such a model should be relatively easy since it is reduced to a linear regression problem after we choose observables from \mathcal{F}_{sub} .

Therefore, the invariance property of the chosen subspace may be considered as a more general characteristic to evaluate the modeling procedure itself than the modeling error $r(x, u)$ defined in (12). In fact, if we change the observables of the Model 2 in the example of Section III-A from $[x_k \ x_k^2 e^{-x_k} \ x_k^2]^T$ to $[\alpha x_k \ \alpha x_k^2 e^{-x_k} \ \alpha x_k^2]^T$ for some $\alpha \in \mathbb{R}$, norms of the modeling error $r(x, u)$ result in different values as shown in Fig. 3 despite the fact that both models should be considered as essentially the same ones since the choices of observables are the same up to multiplicity by α . This result may be also inferred from the following error bounds analysis.

Proposition 3: Let g be observables defined in (27) and suppose μ_x and μ_u are positive measures with compact supports s.t. $(\mathcal{X}, \mathcal{A}_x, \mu_x)$ and $(\mathcal{U}, \mathcal{A}_u, \mu_u)$ are measure spaces

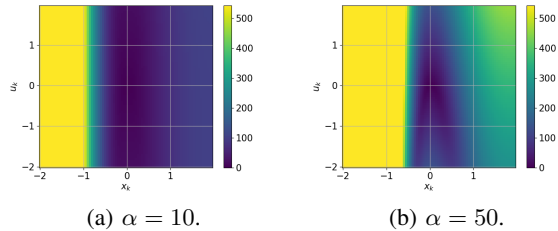


Fig. 3: Heat maps of $\|r(x_k, u_k)\|_2$ of the Model 2 (21) leaned with observables $g(x_k) = [\alpha x_k \quad \alpha x_k^2 e^{-x_k} \quad \alpha x_k^2]^\top$. Also see Fig. 1b for comparison.

with any appropriate σ -algebras \mathcal{A}_x and \mathcal{A}_u , respectively. Also, let $\mu := \mu_x \mu_u$ be their product measure. If g is measurable and continuous, the following holds:

$$\|r\|_{L_2}^2 \leq \|g \circ F\|_{L_2}^2 + \|[A \ B]\| \{ \|[A \ B]\| \|h\|_{L_2}^2 + 2\langle \|(g \circ F)(\cdot)\|_2, \|h(\cdot)\|_2 \rangle_{L_2} \}, \quad (43)$$

where $h : \mathcal{X} \times \mathcal{U} \rightarrow \mathbb{R}^{N+p}$ is a vector-valued function s.t.

$$h(x, u) := \begin{bmatrix} g(x) \\ u \end{bmatrix}, \quad (44)$$

and the function $\|(g \circ F)(\cdot)\|_2 : \mathbb{R}^{n+p} \rightarrow \mathbb{R}_{\geq 0} : (x, u) \mapsto \|(g \circ F)(x, u)\|_2$ denotes an l_2 norm on \mathbb{R}^{n+p} , so does $\|h(\cdot)\|_2$.

Proof: See Appendix B. \blacksquare

Note that the measures μ_x and μ_u in Proposition 3 correspond to probability distributions from which we sample data points x_k and u_k , respectively.

Remark 2: Given a model of the form (11), if we construct another model with the same observables but multiplied by some $\alpha \neq 0$ s.t. $[\alpha x_k^\top \quad \alpha \tilde{g}(x_k)^\top]^\top$, error bounds given by Proposition 3 can be different for these essentially same models. For instance, by replacing B in (11) with αB , both models represent the exact same difference equation up to multiplicity α , while the corresponding error bounds may be different, e.g., $\|g \circ F\|_{L_2}$ and $\|[A \ B]\|$ in (43) become $|\alpha| \|g \circ F\|_{L_2}$ and $\|[A \ \alpha B]\|$, etc.

Thus, it should be emphasized that the modeling error $r(x, u)$ we adopt in this paper is specific to individual learning results and error analyses may not be robust to unessential variations of models. However, it is useful to incorporate into the modeling procedure since it depends on all model parameters and optimization problems can be posed in a natural way based on it, as seen in the loss function $J(g, A, B)$ in (25). Devising characteristics that are both appropriate to measure the accuracy of models and useful to formulate the learning problem is left for future work.

F. Restricting Inputs of the Data Set

In addition to the modification of the initially learned model, we also propose a data sampling strategy that generates the input u_k deterministically such that (u_k, u_{k+1}, \dots) will be a sequence of data points sampled from continuous functions. From the modeling perspective, it is in general advisable to sample data points (x_k, u_k) randomly, i.e., from some probability distribution. Indeed, assuming that data

points (x_k, u_k) are i.i.d. random variables, it is confirmed that minimizing the loss function $J(g, A, B)$ in (25) corresponds to minimizing the norm (13) of the modeling error r since the first term of $J(g, A, B)$ is related to $\|r\|_{L_2}$ as:

$$\frac{1}{M} \|AG_x + BU - G_y\|_F^2 = \frac{1}{M} \sum_{k=1}^M \|r(x_k, u_k)\|_2^2 \xrightarrow{\text{a.s.}} \int_{\mathcal{X} \times \mathcal{U}} \|r(x, u)\|_2^2 dx du \quad (M \rightarrow \infty) = \|r\|_{L_2}^2, \quad (45)$$

where the almost sure convergence follows from the strong law of large numbers.

However, it is often the case that sampling a very large number of data points across the entire space is not practical due to limitations of experimental or computational resources. For non-autonomous systems, the space from which the data (x_k, u_k) is sampled is the product space $\mathcal{X} \times \mathcal{U}$, not the original state space \mathcal{X} , and it is especially difficult to sample enough data in applications. As a result, learned models may be overfitted or biased, which do not necessarily lead to the modeling error profile consistent with the analysis in (45).

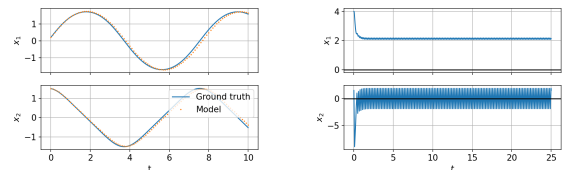
In this paper, we propose to only use deterministic u_k sampled from continuous functions. Since the solution $x(t)$ to (1) is assumed to be continuous and $\tilde{g}(x)$ defined by (29) is also continuous, the control inputs (14) are always discretized points sampled from continuous functions. Hence, for the same reason as that of the modification of the initial model in Section III-D, we only use u_k sampled from continuous functions so that Steps 1 and 2 can minimize losses over possible regime of dynamics realized by the controller (14) only.

IV. NUMERICAL EXAMPLES

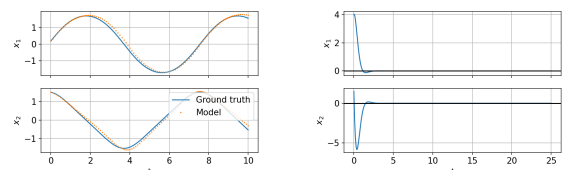
In this section, state-prediction is only implemented with $u_k \equiv 0$ for simplicity. Also, the control objective is defined as stabilizing the system at the origin while minimizing the cost and LQR is used for the controller design.

A. Simple Pendulum

The simple pendulum is considered as the first example:



(a) State prediction of the model trained with (47). (b) Controller performance of the model trained with (47).



(c) State prediction of the model trained with (48). (d) Controller performance of the model trained with (48).

Fig. 4: Results of the simple pendulum.

$$\ddot{\theta} = -\sin \theta + u, \quad (x_1 := \theta, x_2 := \dot{\theta}). \quad (46)$$

We collect 300 data sets generated by (46), each of which consists of a single trajectory of a length of 50 steps with the sampling period $\Delta t = 0.1$ starting from an initial condition $x_0 \sim \text{Uniform}[-3, 3]^2$. The Runge-Kutta method is used to solve (46) with a step size of 0.01. We include one nonlinear feature $\tilde{g}(x_k) \in \mathbb{R}$ ($N = 1$) in the model, which is a neural network with a single hidden layer consisting of 10 neurons and the swish function is used as the activation. Step 1 is implemented in TensorFlow.

The following two types of u_k are considered to evaluate the efficacy of the sampling strategy in Section III-F:

$$u_k \sim \text{Uniform}[-1, 1], \quad (47)$$

$$u_k = \cos(\omega_i k \Delta t), \quad \omega_i := 20i, \quad i = 0, 1, \dots, 5. \quad (48)$$

In the proposed method that adopts (48), each single trajectory data set is split evenly into six groups \mathcal{D}_i and u_k with ω_i is included in \mathcal{D}_i ($i = 0, 1, \dots, 5$).

Figure 4 shows the results of the models obtained by Step 1, where the state predictions (Figs. 4a and 4c) are implemented according to (31) and the control simulations (Figs. 4b and 4d) use LQR gains computed with the cost $\sum_{k=0}^{\infty} 100x_{k,1}^2 + x_{k,2}^2 + u_k^2$. Note that if the discretized dynamics F that is considered as equivalent to the original dynamics (46) can be obtained by the forward Euler discretization, F is linear w.r.t. input and high predictive accuracy is expected by Corollary 1 with the use of sufficiently rich feature maps. Whereas the state-prediction accuracy barely changes with different types of u_k , the controller performance is greatly deteriorated if the model uses the randomly generated input (47). The controller designed for the model trained with the proposed sampling strategy successfully makes the state converge to the origin. Since the control objective is already achieved by the initial model, Step 2 is not applied in this example.

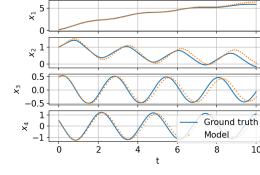
B. Inverted Pendulum on A Cart

The inverted pendulum on a cart is considered as the second example, whose dynamics is given as follows [26]:

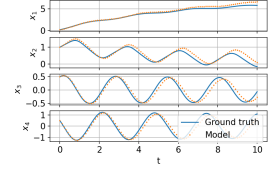
$$\begin{cases} \dot{x}_1 = x_2, \\ \dot{x}_2 = \frac{-m^2 L^2 g \cos x_3 \sin x_3 + mL^2 A(x_2, x_3, x_4) + mL^2 u}{mL^2(M + m(1 - \cos^2 x_3))}, \\ \dot{x}_3 = x_4, \\ \dot{x}_4 = \frac{(m + M)mgL \sin x_3 - mL \cos x_3 A(x_2, x_3, x_4) + mL \cos x_3 u}{mL^2(M + m(1 - \cos^2 x_3))}, \end{cases} \quad (49)$$

where $A(x_2, x_3, x_4) = mLx_4^2 \sin x_3 - \delta x_2$, $m = 1$, $M = 5$, $L = 2$, $g = -10$, and $\delta = 1$. Step 1 is applied with the same conditions as the first example except for the number of hidden layers, which is changed to 25. Also, only the deterministic sampling (48) for u_k is considered in this example. For the controller design, the cost is defined as $\sum_{k=0}^{\infty} 100x_{k,1}^2 + x_{k,2}^2 + 100x_{k,3}^2 + x_{k,4}^2 + u_k^2$. The governing equation (49) can yield its equivalent discretized dynamics as the control-affine form with the forward Euler and Corollary 1 is applicable to the state-prediction with $u_k \equiv 0$.

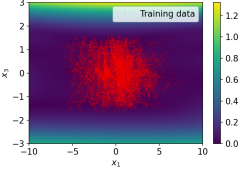
While the initially learned model has reasonable predictive accuracy as in Fig. 5a, the controller performance suffers from the undesirable modeling error effect, which is shown in Fig. 5e. Thus, Step 2 is implemented to modify the model,



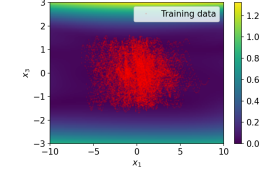
(a) State prediction of the initial model.



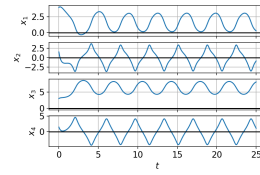
(b) State prediction of the modified model.



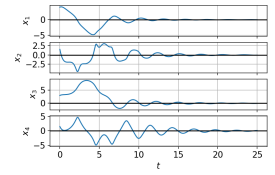
(c) State prediction error of the initial model.



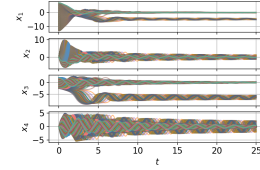
(d) State prediction error of the modified model.



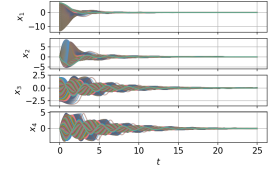
(e) Controller performance of the initial model.



(f) Controller performance of the modified model.



(g) Estimate of basin of attraction of the initial model.



(h) Estimate of basin of attraction of the modified model.

Fig. 5: Results of the inverted pendulum on a cart. (c),(d): x_2 and x_4 are fixed to 0. (g),(h): Tested ranges are $x_1(0) \in [-13, 6.9]$, $x_2(0) \in [-2.5, 2]$ with $x_2(0) = x_4(0) = 0$.

for which we additionally collect data points in the same way as Step 1. The TensorFlow Constrained Optimization module [27] is used to solve the optimization problem in Step 2 with $\epsilon_A = \epsilon_B = 0.1$. The LQR gain is also recomputed with the updated model parameters ($A + \Delta A$, $B + \Delta B$).

It is shown in Fig. 5f that the modified model achieves the control objective. As a more quantitative analysis, we estimate the basin of attraction of the closed-loop systems by testing various initial conditions, whose results are shown in Figs. 5g and 5h. Some initial conditions do not converge to the origin for the closed-loop system formed by the initial model, while it is shown that the given set of initial conditions is a basin of attraction for the one formed by the modified model. Moreover, the modified model retains good state-prediction accuracy thanks to the constraints on ΔA and ΔB and it is comparable to that of the initial model (Figs. 5a and 5b). Finally, the profiles of the state prediction errors are evaluated. Figures 5c and 5d show the heat maps of $\|[I \ 0]r(x, 0)\|_2$ with $x_2 = x_4 = 0$, which are overlaid with the data points used in Step 1. It is confirmed that both models have quite similar error profiles and the good

state-prediction accuracy of the initial model is successfully preserved after the modification.

V. CONCLUSION

A control-aware learning method is proposed along with a simple but effective data sampling strategy for Koopman operator-based control. The initial learning of the observables and the operator matrices is augmented by a second step to improve the controller performance. The use of deterministically-sampled input data from continuous functions improves the controller performance and the proposed two-stage learning contributes to improved closed-loop behavior by updating the operator matrices while retaining high state-prediction accuracy obtained by the initially learned model.

VI. ACKNOWLEDGEMENT

This work was funded by APRA-E under the project *SA-FARI: Secure Automation for Advanced Reactor Innovation*.

APPENDIX

A. Proof of Proposition 1

Suppose $\text{span}(g_1 \cdots, g_D)$ is an invariant subspace under the action of the Koopman operator \mathcal{K} , which implies

$$\mathcal{K}g = \sum_{j=1}^D a_j(\mathcal{K}g_j), \quad (50)$$

is in $\text{span}(g_1 \cdots, g_D)$ for $\forall g \in \text{span}(g_1 \cdots, g_D)$, where $g = \sum_{j=1}^D a_j g_j$ for some $a_j \in \mathbb{R}$. By taking $g = g_i$, $i = 1, \dots, D$, we have

$$\begin{aligned} \exists k_{i1}, \dots, k_{iD} \in \mathbb{R} \text{ s.t. } \mathcal{K}g_i &= \sum_{j=1}^D k_{ij} g_j, \text{ for } i = 1, \dots, D, \\ \Leftrightarrow \exists K \in \mathbb{R}^{D \times D} \text{ s.t. } \begin{bmatrix} \mathcal{K}g_1 \\ \vdots \\ \mathcal{K}g_D \end{bmatrix} &= K \begin{bmatrix} g_1 \\ \vdots \\ g_D \end{bmatrix}. \end{aligned} \quad (51)$$

Conversely, if there exists $K \in \mathbb{R}^{D \times D}$ satisfying (8), for $\forall g = \sum_{i=1}^D a_i g_i \in \text{span}(g_1, \dots, g_D)$,

$$\begin{aligned} \mathcal{K}g &= \sum_{i=1}^D a_i(\mathcal{K}g_i) \\ &= \sum_{i=1}^D a_i \sum_{j=1}^D k_{ij} g_j \text{ (for some } k_{ij} \in \mathbb{R}) \\ &= \sum_{j=1}^D \left(\sum_{i=1}^D a_i k_{ij} \right) g_j \\ &\in \text{span}(g_1, \dots, g_D). \end{aligned} \quad (52)$$

B. Proof of Proposition 3

Since μ_x and μ_u have compact supports and g is both measurable and continuous, $g \in L_p(\mathcal{X}, \mathcal{A}_x, \mu_x)$ for all $1 \leq p < \infty$. Specifically, we have $g \in L_1(\mathcal{X}, \mathcal{A}_x, \mu_x)$ and $g \in$

$L_2(\mathcal{X}, \mathcal{A}_x, \mu_x)$. The function h is well-defined as $h \in L_2$. Indeed,

$$\begin{aligned} &\int_{\mathcal{X} \times \mathcal{U}} \left\| \begin{bmatrix} g(x) \\ u \end{bmatrix} \right\|_2^2 \mu(dxdu) \\ &= \underbrace{\int_{\mathcal{X}} \|g(x)\|_2^2 \mu_x(dx)}_{=:a} \underbrace{\int_{\mathcal{U}} \mu_u(du)}_{=:b} + \underbrace{\int_{\mathcal{X}} \mu_x(dx)}_{=:c} \underbrace{\int_{\mathcal{U}} \|u\|_2^2 \mu_u(du)}_{=:d} \\ &< \infty, \end{aligned} \quad (53)$$

where the last inequality holds since $a = \|g\|_{L_2}^2 < \infty$ and b , c , and d are also finite since the supports of μ_x and μ_u are bounded. Using the triangle inequality, we have

$$\begin{aligned} \|r(x, u)\|_2 &= \left\| g(F(x, u)) - [A \ B] \begin{bmatrix} g(x) \\ u \end{bmatrix} \right\|_2 \\ &\leq \|g(F(x, u))\|_2 + \|[A \ B]\| \left\| \begin{bmatrix} g(x) \\ u \end{bmatrix} \right\|_2, \\ \Leftrightarrow \|r(x, u)\|_2^2 &\leq \|g(F(x, u))\|_2^2 \\ &\quad + \|[A \ B]\| \left\{ \|[A \ B]\| \left\| \begin{bmatrix} g(x) \\ u \end{bmatrix} \right\|_2^2 \right. \\ &\quad \left. + 2\|g(F(x, u))\|_2 \left\| \begin{bmatrix} g(x) \\ u \end{bmatrix} \right\|_2 \right\}. \end{aligned} \quad (54)$$

Define

$$\hat{h} : \mathcal{X} \times \mathcal{U} \rightarrow \mathbb{R}^{n+p} : (x, u) \mapsto [A \ B] \begin{bmatrix} g(x) \\ u \end{bmatrix}. \quad (55)$$

It is confirmed that $\hat{h} \in L_2$ as

$$\begin{aligned} &\int_{\mathcal{X} \times \mathcal{U}} \left\| [A \ B] \begin{bmatrix} g(x) \\ u \end{bmatrix} \right\|_2^2 \mu(dxdu) \\ &= \int_{\mathcal{X} \times \mathcal{U}} \sum_{i=1}^N \left(\sum_{l=1}^N a_{i,l} g_l(x) + \sum_{l=1}^p b_{i,l} u_l \right)^2 \mu(dxdu) \\ &= \sum_{i=1}^N \left\{ \sum_{l=1}^N a_{i,l}^2 \|g_l\|_{L_2}^2 \int_{\mathcal{U}} \mu_u(du) \right. \\ &\quad + 2 \sum_{j=2}^N \sum_{l=1}^{j-1} a_{i,l} a_{i,j} \langle g_l, g_j \rangle_{L_2} \int_{\mathcal{U}} \mu_u(du) \\ &\quad + 2 \sum_{l=1}^N \sum_{j=1}^p a_{i,l} b_{i,j} \int_{\mathcal{X}} g_l(x) \mu_x(dx) \int_{\mathcal{U}} u_j \mu_u(du) \\ &\quad + \sum_{l=1}^p b_{i,l}^2 \int_{\mathcal{X} \times \mathcal{U}} u_l^2 \mu(dxdu) \\ &\quad \left. + 2 \sum_{j=2}^p \sum_{l=1}^{j-1} b_{i,l} b_{i,j} \int_{\mathcal{X} \times \mathcal{U}} u_l u_j \mu(dxdu) \right\} \end{aligned} \quad (56)$$

$< \infty$,

(57)

where any integration in (56) is finite since the supports of μ_x and μ_u are bounded and $g \in L_1$, i.e., g is integrable. Noticing that r is a linear combination of $g \circ F \in L_2$ and $\hat{h} \in L_2$, we have $r \in L_2$ by the same argument as above.

Also, l_2 norms:

$$N_1(\cdot) := \|(g \circ F)(\cdot)\|_2 : \mathbb{R}^{n+p} \rightarrow \mathbb{R}_{\geq 0} \\ : (x, u) \mapsto \|(g \circ F)(x, u)\|_2, \quad (58)$$

$$N_2(\cdot) := \|h(\cdot)\|_2 : \mathbb{R}^{n+p} \rightarrow \mathbb{R}_{\geq 0} : (x, u) \mapsto \|h(x, u)\|_2, \quad (59)$$

belong to L_2 as

$$\int_{\mathcal{X} \times \mathcal{U}} |N_1(x, u)|^2 \mu(dxdu) = \int_{\mathcal{X} \times \mathcal{U}} \|(g \circ F)(x, u)\|_2^2 \mu(dxdu) \\ = \|g \circ F\|_{L_2}^2 \\ < \infty, \quad (60)$$

$$\int_{\mathcal{X} \times \mathcal{U}} |N_2(x, u)|^2 \mu(dxdu) = \int_{\mathcal{X} \times \mathcal{U}} \|h(x, u)\|_2^2 \mu(dxdu) \\ = \|h\|_{L_2}^2 \\ < \infty, \quad (61)$$

so that the following quantity is well-defined as the inner product of L_2 :

$$\int_{\mathcal{X} \times \mathcal{U}} \|g(F(x, u))\|_2 \left\| \begin{bmatrix} g(x) \\ u \end{bmatrix} \right\|_2 dxdu \\ = \langle \|(g \circ F)(\cdot)\|_2, \|h(\cdot)\|_2 \rangle_{L_2}. \quad (62)$$

Therefore, (54) implies the following:

$$\|r\|_{L_2}^2 = \int_{\mathcal{X} \times \mathcal{U}} \|r(x, u)\|_2^2 dxdu \\ \leq \int_{\mathcal{X} \times \mathcal{U}} \|g(F(x, u))\|_2^2 dxdu \\ + \|[A \ B]\| \left\{ \|[A \ B]\| \int_{\mathcal{X} \times \mathcal{U}} \left\| \begin{bmatrix} g(x) \\ u \end{bmatrix} \right\|_2^2 dxdu \right. \\ \left. + 2 \int_{\mathcal{X} \times \mathcal{U}} \|g(F(x, u))\|_2 \left\| \begin{bmatrix} g(x) \\ u \end{bmatrix} \right\|_2 dxdu \right\} \\ = \|g \circ F\|_{L_2}^2 + \|[A \ B]\| \left\{ \|[A \ B]\| \|h\|_{L_2}^2 \right. \\ \left. + 2 \langle \|(g \circ F)(\cdot)\|_2, \|h(\cdot)\|_2 \rangle_{L_2} \right\}. \quad \blacksquare$$

REFERENCES

- [1] C. Rowley, I. Mezić, S. Bagheri, P. Schlatter, and D. S. Henningson, "Spectral analysis of nonlinear flows," *Journal of Fluid Mechanics*, vol. 641, pp. 115–127, 2009.
- [2] P. Schmid and J. Sesterhenn, "Dynamic mode decomposition of numerical and experimental data," in *Sixty-First Annual Meeting of the APS Division of Fluid Dynamics*, 2008.
- [3] M. Williams, I. Kevrekidis, and C. Rowley, "A data driven approximation of the Koopman operator: Extending dynamic mode decomposition," *Journal of Nonlinear Science*, vol. 25, no. 6, pp. 1307–1346, 2015.
- [4] G. Mamakoukas, M. L. Castaño, X. Tan, and T. D. Murphey, "Derivative-based Koopman operators for real-time control of robotic systems," *IEEE Transactions on Robotics*, vol. 37, no. 6, pp. 2173–2192, 2021.
- [5] G. Mamakoukas, M. Castano, X. Tan, and T. Murphey, "Local Koopman operators for data-driven control of robotic systems," in *Proceedings of the Robotics: science and systems*, 2019.
- [6] D. A. Haggerty, M. J. Banks, P. C. Curtis, I. Mezić, and E. W. Hawkes, "Modeling, Reduction, and Control of a Helically Actuated Inertial Soft Robotic Arm via the Koopman Operator," *arXiv e-prints*, p. arXiv:2011.07939, 2020.
- [7] M. Korda and I. Mezić, "Linear predictors for nonlinear dynamical systems: Koopman operator meets model predictive control," *Automatica*, vol. 93, pp. 149–160, 2018.
- [8] A. Narasingam and J. S.-I. Kwon, "Koopman Lyapunov-based model predictive control of nonlinear chemical process systems," *AICHE Journal*, vol. 65, no. 11, p. e16743, 2019.
- [9] S. Peitz, S. E. Otto, and C. W. Rowley, "Data-driven model predictive control using interpolated Koopman generators," *SIAM Journal on Applied Dynamical Systems*, vol. 19, no. 3, pp. 2162–2193, 2020.
- [10] D. Bruder, B. Gillespie, C. D. Remy, and R. Vasudevan, "Modeling and Control of Soft Robots Using the Koopman Operator and Model Predictive Control," *arXiv e-prints*, p. arXiv:1902.02827, 2019.
- [11] X. Zhang, W. Pan, R. Scattolini, S. Yu, and X. Xu, "Robust tube-based model predictive control with Koopman operators," *Automatica*, vol. 137, p. 110114, 2022.
- [12] S. H. Son, A. Narasingam, and J. Sang-II Kwon, "Handling plant-model mismatch in Koopman Lyapunov-based model predictive control via offset-free control framework," *arXiv e-prints*, p. arXiv:2010.07239, 2020.
- [13] N. Kochdumper and S. Bak, "Conformant synthesis for Koopman operator linearized control systems," in *2022 IEEE 61st Conference on Decision and Control*, pp. 7327–7332, 2022.
- [14] M. Korda and I. Mezić, "On convergence of extended dynamic mode decomposition to the Koopman operator," *Journal of Nonlinear Science*, vol. 28, no. 2, pp. 687–710, 2018.
- [15] J. L. Proctor, S. L. Brunton, and J. N. Kutz, "Dynamic mode decomposition with control," *SIAM Journal on Applied Dynamical Systems*, vol. 15, no. 1, pp. 142–161, 2016.
- [16] J. L. Proctor, S. L. Brunton, and J. N. Kutz, "Generalizing koopman theory to allow for inputs and control," *SIAM Journal on Applied Dynamical Systems*, vol. 17, no. 1, pp. 909–930, 2018.
- [17] I. Abraham, G. De La Torre, and T. Murphey, "Model-based control using Koopman operators," in *Proceedings of the Robotics: Science and Systems*, 2017.
- [18] S. Peitz and S. Klus, "Koopman operator-based model reduction for switched-system control of PDEs," *Automatica*, vol. 106, pp. 184–191, 2019.
- [19] D. Uchida, A. Yamashita, and H. Asama, "Data-driven Koopman controller synthesis based on the extended \mathcal{H}_2 norm characterization," *IEEE Control Systems Letters*, vol. 5, no. 5, pp. 1795–1800, 2021.
- [20] S. Klus, P. Koltai, and C. Schütte, "On the numerical approximation of the Perron-Frobenius and Koopman operator," *Journal of Computational Dynamics*, vol. 3, no. 1, pp. 51–79, 2016.
- [21] E. Yeung, S. Kundu, and N. Hodas, "Learning deep neural network representations for Koopman operators of nonlinear dynamical systems," *Proceedings of the 2019 American Control Conference (ACC)*, pp. 4832–4839, 2019.
- [22] N. Takeishi, Y. Kawahara, and T. Yairi, "Learning Koopman invariant subspaces for dynamic mode decomposition," *Advances in Neural Information Processing Systems*, vol. 30, pp. 1130–1140, 12 2017.
- [23] S. Pan and K. Duraisamy, "Physics-informed probabilistic learning of linear embeddings of nonlinear dynamics with guaranteed stability," *SIAM Journal on Applied Dynamical Systems*, vol. 19, no. 1, pp. 480–509, 2020.
- [24] Y. Han, W. Hao, and U. Vaidya, "Deep learning of Koopman representation for control," in *Proceedings of the 2020 59th IEEE Conference on Decision and Control (CDC)*, pp. 1890–1895, 2020.
- [25] J. C. Schulze, D. T. Doncevic, and A. Mitsos, "Identification of MIMO Wiener-type Koopman models for data-driven model reduction using deep learning," *Computers & Chemical Engineering*, vol. 161, p. 107781, 2022.
- [26] S. L. Brunton and J. N. Kutz, *Data-Driven Science and Engineering: Machine Learning, Dynamical Systems, and Control*. Cambridge University Press, 2019.
- [27] A. Cotter, H. Jiang, and K. Sridharan, "Two-player games for efficient non-convex constrained optimization," in *Proceedings of the 30th International Conference on Algorithmic Learning Theory*, vol. 98, pp. 300–332, 2019.